PAPER

Detectability of the chiral gravitational wave background from audible axions with the LISA-Taiji network

Commun. Theor. Phys. **77** (2025) 115403 (14pp)
https://doi.org/10.1088/1572-9494/add1b9
CSTR: 32041.14.CTPadd1b9

Detectability of the chiral gravitational wave background from audible axions with the LISA-Taiji network

Hong Su[1,2,3], Baoyu Xu[4,5], Ju Chen[2,6,*], Chang Liu[7,*] and Yun-Long Zhang[1,4,*]

[1] School of Fundamental Physics and Mathematical Sciences, Hangzhou Institute for Advanced Study, UCAS, Hangzhou 310024, China
[2] Taiji Laboratory for Gravitational Wave Universe (Beijing/Hangzhou), University of Chinese Academy of Sciences, Beijing 100049, China
[3] CAS Key Laboratory of Theoretical Physics, Institute of Theoretical Physics, Chinese Academy of Sciences, Beijing 100190, China
[4] National Astronomical Observatories, Chinese Academy of Sciences, Beijing 100101, China
[5] School of Astronomy and Space Science, University of Chinese Academy of Sciences, Beijing 100049, China
[6] International Center for Theoretical Physics Asia-Pacific (ICTP-AP), University of Chinese Academy of Sciences, Beijing 100190, China
[7] Center for Gravitation and Cosmology, College of Physical Science and Technology, Yangzhou University, Yangzhou 225009, China

E-mail: chenju@ucas.ac.cn, liuchang@yzu.edu.cn and zhangyunlong@nao.cas.cn

Received 28 March 2025, revised 23 April 2025
Accepted for publication 29 April 2025
Published 4 July 2025

Abstract

The chiral gravitational wave background (GWB) can be produced by axion-like fields in the early universe. We perform parameter estimation for two types of chiral GWB with the LISA-Taiji network: axion-dark photon coupling and axion-Nieh–Yan coupling. We estimate the spectral parameters of these two mechanisms induced by the axion and determine the normalized model parameters using the Fisher information matrix. For highly chiral GWB signals that we choose to analyze in the mHz band, the normalized model parameters are constrained with a relative error less than 6.7% (dark photon coupling) and 2.2% (Nieh–Yan coupling) at the one-sigma confidence level. The circular polarization parameters are constrained with a relative error around 21% (dark photon coupling) and 6.2% (Nieh–Yan coupling) at the one-sigma confidence level.

Keywords: LISA-taiji network, chiral gravitational wave background, audible axion

(Some figures may appear in colour only in the online journal)

1. Introduction

The direct detection [1] of gravitational waves (GWs) by the Laser Interferometer Gravitational-Wave Observatory (LIGO) [2] has offered a novel method for exploring the physics of the early Universe [3–6]. GWs produced by axions or axion-like particles (ALPs), especially the stochastic gravitational wave background (SGWB) from the early Universe, enable the detection of new physics beyond the Standard Model and provide insights into the early Universe [7–14]. Axions were originally introduced to address the strong CP problem within the Standard Model [15–20]. While numerous mechanisms exist for the production of axions in the early Universe [21, 22], enabling a wide range of dark matter axion masses, these mechanisms may also contribute to various cosmological phenomena [23].

* Authors to whom any correspondence should be addressed.

Axions and ALPs typically have weak couplings to photons or other Standard Model particles, making them difficult to detect directly [24, 25]. Moreover, these particles have been proposed to address other Standard Model and cosmological challenges, such as resolving the electroweak hierarchy problem [26, 27], serving as dark matter (DM) candidates [24, 28, 29] or inflatons [30], and being present in string theory frameworks [31]. The audible axions model proposed in [32, 33] describes the coupling between axions and dark photons (gauge bosons), in which dark photons experience tachyonic instability when axions oscillate. The model postulates that axions or ALPs possess large initial velocities, enabling the generation of detectable GW signals even with small decay constants. This process results in the generation of an SGWB in the early Universe, allowing us to detect these particles, which carry chirality. Parity violation will serve as a powerful observable for distinguishing cosmological background GWs from astrophysical ones [34]. Probing axion dark matter through future space-based gravitational-wave detectors will enable the exploration of broader parameter space for axions and ALPs. Except for the ground-based gravitational-wave observatories [35, 36], forthcoming space-based missions hold the potential to probe axion-like dark matter directly [37–39].

The SGWB arises from the superposition of GWs produced by a large number of independent sources [40]. It exhibits stochasticity and has a signal strength that is relatively weak compared to the total intensity sensitivity of detectors, categorizing it as a weak signal, and methods for its detection have been developed [41]. Due to the stochastic and uncorrelated nature of the general generation process, the SGWB is assumed to be unpolarized. However, parity violation in gravity, such as the Chern–Simons coupling [42, 43] and the Nieh–Yan coupling in teleparallel equivalent of general relativity (TEGR) [44–52], can modify the generation and propagation of gravitational waves, leading to a circularly polarized SGWB. The chirality of GWs can be effectively measured by several detectors, including ground-based interferometers [53–55]. While current ground-based detectors are insufficiently sensitive to constrain circular polarization significantly [56, 57], more precise measurements are expected in the coming years [58]. For space-based detection, the LISA-Taiji network [59–61] offers a promising approach due to its non-coplanar configuration. Additionally, Cosmic Microwave Background (CMB) observations [62, 63] provide an independent probe of circular polarization through primordial B-mode signatures.

LISA (Laser Interferometer Space Antenna) is a triangular GW detector in the orbit around the Sun, which is expected to be launched in the 2030s, with an arm length of $L = 2.5 \times 10^9$m [64]. Taiji is similar to LISA but has an arm length of $L = 3 \times 10^9$m [65]. Due to their planar configuration, individual detectors are insensitive to the chiral signatures of GWs. For an isotropic SGWB, the detection of its circular polarization requires the correlation of two non-coplanar gravitational wave detectors [66]. Therefore, a network of detectors is necessary, such as ground-based networks [67, 68] or the space-based network LISA-Taiji [61, 69–76], which can enhance the detection of the circular polarization of the SGWB. Furthermore, space-based GW detector networks also provide numerous other advantages, including improved gravitational wave polarization measurements [77], enhanced parameter estimation for Galactic binaries [78], better sky localization accuracy [79, 80], more accurate localization of massive binaries [81], detection of black hole formation mechanisms [82], increased detection capabilities for stellar binary black holes [83], and increased precision of GW standard sirens and cosmological parameter estimation [84–86].

To evaluate the detection capability of the LISA-Taiji network for chiral gravitational wave background (GWB), we estimate the spectral parameters and normalized model parameters of the chiral GWB generated by early cosmic axions using the Fisher information matrix. Additionally, we perform a Fisher analysis based on the fitted SGWB energy density spectrum from the dark photon coupling model [87] and broken power-law spectrum from the Nieh–Yan coupling model [52].

The paper is organized as follows. In section 2, we briefly introduce how axions generate chiral gravitational waves through coupling with dark photons or the Nieh-–term, and present the energy density spectrum of the resulting gravitational waves, along with fitted templates and parameters. In section 3, we describe the configuration of the space-based GW detector network and calculate its response to GWs. In section 4, we derive the Fisher information matrix and determine the parameters for two different GW energy spectra with the network. In section 5, we present the conclusion and discussion. The calculations in this work are performed using the Python packages `numpy` and `scipy`, and the plots are generated using `matplotlib` and `GetDist`.

2. Audible axions and chiral GW background

Several mechanisms that produce chiral GWs from audible axions have been explored in prior research. One is the coupling of axion to dark photon [32, 87, 88], while the other involves axion coupling to the parity-violating gravity such as Chern–Simons [89–91] and Nieh–Yan modified gravity [44–52]. The former just generates chiral GWs mediated by dark photons, while the latter can produce GWs directly and efficiently. In this section, we explore the GW spectrum template and fitting parameters produced by these mechanisms.

2.1. Chiral GWB from dark photon coupling

The chiral GWB can be generated through the asymmetrical production of dark photons [32, 87, 88]. In this mechanism, the total action can be expressed as

$$S_{\rm DP} = \int {\rm d}^4x\sqrt{-g}\left[\frac{M_p^2}{2}R - \frac{1}{4}X_{\mu\nu}X^{\mu\nu} + \frac{\alpha_X}{4f_X}\phi X_{\mu\nu}\widetilde{X}^{\mu\nu} - \frac{1}{2}\partial_\mu\phi\partial^\mu\phi - V(\phi)\right]. \tag{1}$$

Here, f_X is the decay constant of the axion, α_X is the coupling coefficient and $V(\phi) = m^2 f_X^2\left[1 - \cos\left(\frac{\phi}{f_X}\right)\right]$ is the cosine-

like potential with the axion mass m. The third term in this action leads to a nontrivial dispersion relation for the helicities of dark photons, which takes the form $\omega_{X,\pm}^2 = k_X^2 \mp k_X \frac{\alpha_X}{f_X}\phi'$. This indicates that the asymmetric production of dark photons results in an oscillating stress-energy distribution that sources gravitational waves.

Previous studies provide a well-fitting curve for the chiral gravitational wave energy density spectrum produced by dark photons. For the SGWB template, a suitable ansatz is [87]

$$\tilde{\Omega}_{\rm GW}(\tilde{f}_p) = \frac{\mathcal{A}_s(\tilde{f}_p/f_s)^p}{1 + (\tilde{f}_p/f_s)^p \exp\left[\gamma(\tilde{f}_p/f_s - 1)\right]}, \tag{2}$$

where $\tilde{\Omega}_{\rm GW} \equiv \Omega_{\rm GW}(f)/\Omega_{\rm GW}(f_p)$ represents the normalized GW energy density, f_p denotes the peak frequency. f denotes the GW frequency and $\tilde{f}_p \equiv f/f_p$ is the dimensionless normalized frequency. Moreover, $\mathcal{A}_s$, f_s, γ, p are the fitting parameters.

From the derivation in [32], the peak amplitude and peak frequency of the GW spectrum, at the time of GW emission, are given by $f_p \simeq (\alpha_X\theta)^{2/3} m$, $\Omega_{\rm GW}(f_p) \simeq \left(\frac{f_X}{M_P}\right)^4 \left(\frac{\theta^2}{\alpha_X}\right)^{\frac{4}{3}}$. Here, θ is the initial misalignment angle and $M_P \simeq 2.4 \times 10^{18}\,\mathrm{GeV}$ is the reduced Planck mass. Considering the expansion of the Universe, which leads to redshifting, these quantities become [32]

$$f_p^0 \simeq (\alpha_X\theta)^{2/3}\, T_0 \left(\frac{g_{s,0}}{g_{s,*}}\right)^{1/3} \left(\frac{m}{M_P}\right)^{1/2}, \tag{3}$$

$$\Omega_{\rm GW}^0(f_p^0) \simeq 1.67 \times 10^{-4} g_{s,*}^{-1/3} \left(\frac{f_X}{M_P}\right)^4 \left(\frac{\theta^2}{\alpha_X}\right)^{\frac{4}{3}}. \tag{4}$$

Here, we choose the effective number of relativistic degrees of freedom $g_{s,*} = 106.75$, because the mechanism occurs near the QCD phase transition. $g_{s,0} = 3.938$ is the effective relativistic degree of freedom today when the temperature $T_0 = 2.35 \times 10^{-13}$ GeV. Based on the equations above, to produce detectable GW signals within the mHz frequency band, we adopt the following parameter values: $m = 1.0 \times 10^{-2}$ eV, $f_X = 1.0 \times 10^{17}$ GeV, $\alpha_X = 55$, and $\theta = 1.2$, as proposed by [32].

2.2. Chiral GWB from Nieh–Yan coupling

The chiral GWB can also be generated through an axion-like mechanism that couples to the Nieh–Yan term, resulting in the direct and efficient production of chiral GWB during the radiation-dominated epoch [52]. This generation arises from the tachyonic instability of gravitational perturbations induced by the Nieh–Yan term. The total action for this mechanism can be written as

$$S_{\rm NY} = \int {\rm d}^4x\sqrt{-g}\left[-\frac{M_{\rm p}^2}{2}\hat{T} + \frac{\alpha_T M_{\rm p}^2}{4f_T}\phi\hat{T}_{A\mu\nu}\widetilde{T}^{A\mu\nu} - \frac{1}{2}\partial_\mu\phi\partial^\mu\phi - V(\phi)\right]. \tag{5}$$

Here, $\hat{T}$ is the torsion scalar, which is dynamically equivalent to the Ricci scalar in general relativity. Similar to the action in equation (1), f_T is the axion decay constant, α_T is the coupling coefficient and $V(\phi)$ represents the cosine-like potential. The second term in equation (5) can also lead to a nontrivial dispersion relation for the GW helicities, given by $\omega_{T,\pm}^2 = k_T^2 \pm \frac{\alpha_T\phi'}{f_T M_P^2}k_T$. The k_T here is the wave vector for GWs, indicating that the last term produces an effect analogous to the term $\frac{\alpha_X}{4f_X}\phi X_{\mu\nu}\widetilde{X}^{\mu\nu}$ in the dark photon case.

Specifically, when the axion field oscillates, one of the GW helicities will have a range of modes with imaginary frequencies, resulting in a tachyonic instability that drives exponential growth. Since the growth rate is related to helicities, the left-handed and right-handed GWs are generated asymmetrically, ultimately leading to chiral GWB. In [52], the broken power-law template provides a better fit for the GW spectrum in this model, which can be written as

$$\tilde{\Omega}_T = (\tilde{f}_c)^{\alpha_1}[1 + 0.75(\tilde{f}_c)^{\Delta}]^{\frac{(\alpha_2-\alpha_1)}{\Delta}}. \tag{6}$$

Here, $\tilde{\Omega}_T \equiv \Omega_T(f)/\Omega_c$, where Ω_c is the characteristic energy density. $\tilde{f}_c \equiv f/f_c$ is the dimensionless normalized frequency with the characteristic frequency f_c. Moreover, α_1, α_2 and Δ are fitting parameters.

In this equation, the characteristic frequency today, f_c^0, can be expressed in terms of physical parameters as

$$f_c^0 = 0.7125\,\mathrm{mHz}\left(\frac{100}{g_{s,*}}\right)^{\frac{1}{12}}\left(\frac{9}{14}\alpha_T\theta\right)^{\frac{2}{3}}\left(\frac{m}{\mathrm{eV}}\right)^{\frac{1}{2}}. \tag{7}$$

Here, we also choose $g_{s,*} = 106.75$, as this mechanism occurs near the QCD phase transition. The characteristic energy density Ω_c^0 can similarly be written in terms of physical parameters as

$$\Omega_c^0 = \frac{\theta^2 f_T^2/2}{3M_P^2}\frac{m^2}{H_{\rm osc}^2} \simeq \left(\frac{\theta f_T}{M_P}\right)^2. \tag{8}$$

For the Nieh–Yan coupling model, we choose the following parameters to generate detectable gravitational wave signals in the mHz band: $m = 0.1$ eV, $f_T = 1.0 \times 10^{17}$ GeV, $\alpha_T = 35.61$, and $\theta = 1$ [52].

Due to the axion-like terms, the symmetry between left- and right-handed polarizations allows for spontaneous symmetry breaking, resulting in one chirality dominating. While our analysis focuses on right-handed polarization dominance with positive V, the formalism applies equally to left-handed polarization with negative V. Our choice of polarization sign with $V > 0$ does not affect the generality of results, as the Fisher matrix depends only on the polarization magnitude. In figure 1, we present the broken power-law fit curves of the chirality-dominated SGWB spectrum generated by the dark photon coupling model [32], and the Nieh–Yan coupling model [52].

3. Network of space-based GW detectors

In this section, we adopt the commonly used orbits of LISA and Taiji, combining them to evaluate their effectiveness in detecting the SGWB. We establish the coordinate system in the Solar System Barycentric Coordinate System (SSB).

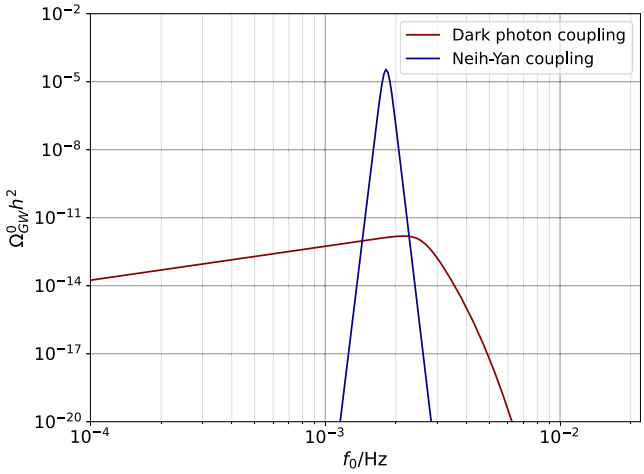

Figure 1. The broken power-law fitted curves of the SGWB for the dark photon (red) and Nieh–Yan (blue) coupling models, each using two parameter sets as described in sections 2.1 and 2.2.

LISA trails the Earth by 20 degrees, and Taiji leads by the same degree, with both detector planes tilted 60 degrees relative to the ecliptic plane. The LISA-Taiji network configuration is displayed as figure 2.

3.1. Noise and sensitivity of the detectors

Each detector contains three interferometers that simultaneously detect the Doppler shift induced by GWs. The data stream of Time-Delay Interferometry (TDI) channel i is given by

$$d_i(t) = s_i(t) + n_i(t), \tag{9}$$

where $s_i(t)$ represents the signal and $n_i(t)$ denotes the instrumental noise. In general, it is more convenient to work in the frequency domain

$$\tilde{d}_i(f) = \int_{-T/2}^{T/2} \mathrm{d}t\, \mathrm{e}^{2\pi i f t} d_i(t), \tag{10}$$

where T represents the observation time. In this paper, we assume that the noise is Gaussian and uncorrelated. The respective correlations of the signal and noise in the frequency domain can be expressed as

$$\begin{aligned}\langle \tilde{s}_i(f)\tilde{s}_j^*(f')\rangle &= \frac{1}{2}S_{ij}(f)\delta(f-f'),\\ \langle \tilde{n}_i(f)\tilde{n}_j^*(f')\rangle &= \frac{1}{2}N_i(f)\delta_{ij}\delta(f-f'),\end{aligned} \tag{11}$$

where $S_{ij}(f)$ and $N_i(f)$ are the one-sided signal and noise power spectral density (PSD), respectively. Assuming independent TDI channel noises (e.g., in the A, E, T combination, which are the optimal TDI variables for LISA-like detectors), $S_{ij}(f)$ can be expressed as

$$\begin{aligned}S_{ij}(f) &= \sum_\lambda P_\lambda(f)\Gamma_{ij}^\lambda(f) = \sum_\lambda P_\lambda(f)\\ &\times [(2\pi kL_i)(2\pi kL_j)W(kL_i)W^*(kL_j)\tilde{\Gamma}_{ij}^\lambda(f) + \text{h.c.}].\end{aligned} \tag{12}$$

Here, $k = f/c$, $\lambda = L$ or R identifies left- and right-handed polarizations, L_i and L_j are the detector arm lengths, $\Gamma_{ij}^\lambda(f)$ is the full detector response function and $P_\lambda(f)$ is the GW power spectrum. The function $W(kL)$ represents the phase delay due to the detector arm length, as detailed in appendix A.2. $\tilde{\Gamma}_{ij}^\lambda(k)$ denotes the geometrical contribution to the detector response function for the correlation between channels i and j, as detailed in equation (A11).

In this work, we adopt the standard two-parameter noise model used for LISA, which accounts for the two dominant noise sources in space-based GW detectors: acceleration (acc) noise and Optical Measurement System (OMS) noise. For Taiji, we use a similar noise model with distinct parameters $A_{\rm acc}$ and $A_{\rm OMS}$. The acceleration noise power spectrum $P_{\rm acc}(f)$ and OMS noise power spectrum $P_{\rm OMS}(f)$ are given by [92, 93]

$$\begin{aligned}P_{\rm acc}(f) &= A_{\rm acc}^2\left[1+\left(\frac{0.4\text{mHz}}{f}\right)^2\right]\left(\frac{2\pi f}{c}\right)^2\\ &\times\left[1+\left(\frac{f}{8\text{mHz}}\right)^4\right]\left(\frac{1}{2\pi f}\right)^4,\end{aligned} \tag{13}$$

$$P_{\rm OMS}(f) = A_{\rm OMS}^2\left[1+\left(\frac{2\text{mHz}}{f}\right)^4\right]\left(\frac{2\pi f}{c}\right)^2. \tag{14}$$

Here, $A_{\rm acc}$ and $A_{\rm OMS}$ are the amplitudes of the acceleration noise and the OMS noise, respectively. For the two detectors, the noise amplitude parameters for LISA [94] and Taiji [70, 95, 96] are listed in table 1.

For convenience, we define the detector's characteristic frequency as $f_* \equiv c/2\pi L$. The power spectral density of the noise for a single detector channel is then given by [13, 97]

$$\begin{aligned}&N_{\rm A}(f) = N_{\rm E}(f)\\ &= 8\sin^2\left(\frac{f}{f_*}\right)\left\{4\left[1+\cos\left(\frac{f}{f_*}\right)+\cos^2\left(\frac{f}{f_*}\right)\right]\right.\\ &\left.\times P_{\rm acc}(f)+\left[2+\cos\left(\frac{f}{f_*}\right)\right]\times P_{\rm OMS}(f)\right\},\end{aligned} \tag{15}$$

and

$$\begin{aligned}N_{\rm T}(f) &= 16\sin^2\left(\frac{f}{f_*}\right)\left\{2\left[1-\cos\left(\frac{f}{f_*}\right)\right]^2\right.\\ &\left.\times P_{\rm acc}(f)+\left[1-\cos\left(\frac{f}{f_*}\right)\right]\times P_{\rm OMS}(f)\right\},\end{aligned} \tag{16}$$

where the subscripts A, E, and T denote the noise-orthogonal TDI channels A, E, and T, respectively. The space-based detector with three equal arms combines into three independent channels: A, E, and T. The A and E channels function as orthogonal interferometers sensitive to GW polarizations. Although their responses differ for GWs from specific directions, the all-sky averaged sensitivities of A and E channels are identical due to the detector's rotational symmetry. As shown in figure 3(a), the T channel (Sagnac combination) remains insensitive to GWs at low frequencies while maintaining

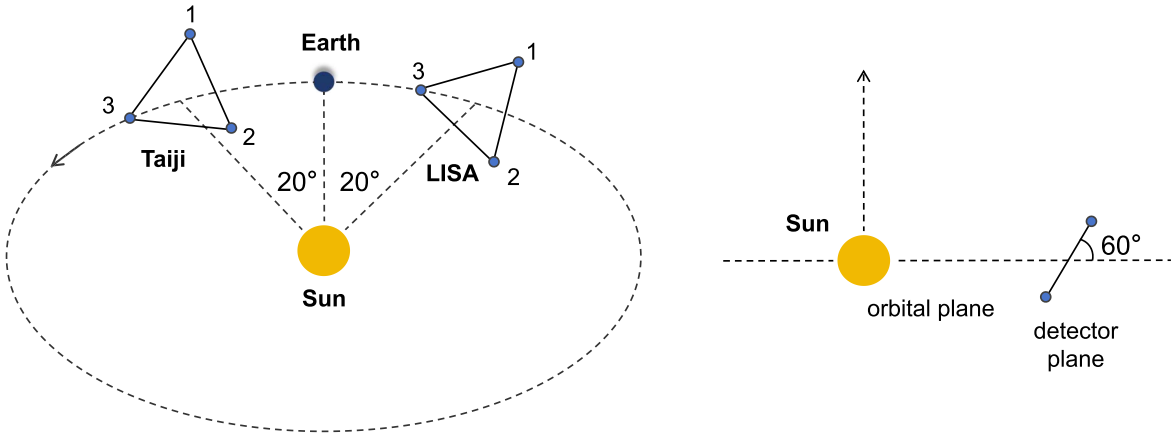

Figure 2. The configuration of the LISA-Taiji joint network, including the spacecraft numbering scheme. LISA orbits 20 degrees behind the Earth, while Taiji precedes the Earth by the same angle. Both detector planes are inclined at 60 degrees relative to the ecliptic plane.

Table 1. Noise amplitude spectral density parameters and arm lengths for different space-based GW detectors.

	$A_{\rm OMS}$	$A_{\rm acc}$	L
LISA	15 pm/$\sqrt{\rm Hz}$	3 fm/s^2/$\sqrt{\rm Hz}$	2.5 Gm
Taiji	8 pm/$\sqrt{\rm Hz}$	3 fm/s^2/$\sqrt{\rm Hz}$	3.0 Gm

sensitivity to instrumental noise. This characteristic allows the T channel to help characterize and subtract instrumental noise, enhancing the overall detection capability, particularly for stochastic background measurements.

To directly compare incident GW signals with detector noise, we define the strain sensitivity of total intensity for all GW modes as [13]

$$P_{N,ii}(f) = \frac{N_i(f)}{\Gamma_{ii}(f)}\,, \tag{17}$$

where $\Gamma_{ii}(f)$ represents the sky-averaged response functions of individual TDI channels, which can be calculated via equation (A14). The corresponding total intensity, in GW energy density units, is given by:

$$h^2\Omega_{N,ii}(f) = \frac{4\pi^2 f^3}{3(H_0/h)^2} P_{N,ii}(f)\,, \tag{18}$$

where $H_0 = h\,100\,{\rm km\,s^{-1}\,Mpc^{-1}}$ is the value of the present-day Hubble parameter and $h = 0.67$ is the dimensionless Hubble parameter. Figure 3 shows the total intensity sensitivity curves for the A and E channels of both LISA and Taiji. Similarly, the SGWB adopts a similar notation, with $P_{N,ij}$ replaced by the GW power spectrum [61]

$$h^2\Omega^{\lambda}_{\rm GW}(f) = \frac{4\pi^2 f^3}{3(H_0/h)^2} P_{\lambda}(f)\,. \tag{19}$$

3.2. LISA-taiji cross-correlations

Individual detectors like LISA or Taiji are insensitive to GW chiral signatures due to their planar configuration. The three arms of LISA form a plane, and this geometry inherently lacks sensitivity to isotropic chiral GWB. For example, left-handed circularly polarized signals of equal intensity from opposite directions incident on the detector plane would cancel their chiral signatures. Taiji, with a similar configuration, shares this limitation. However, when two spatially separated detectors form a non-coplanar network, the combined system gains sensitivity to the Stokes V parameter, characterizing GW chirality. This non-coplanar configuration of the LISA-Taiji network enables detection of isotropic chiral GWB that remains undetectable by individual detectors.

We use the Stokes parameters $I(f)$ and $V(f)$ to characterize the polarization of the SGWB in the cross-correlated detector data stream. They are defined as

$$I(f) = P_R(f) + P_L(f), \quad V(f) = P_R(f) - P_L(f). \tag{20}$$

Here, I represents the total intensity of the GW, while V quantifies the difference between right-handed and left-handed circular polarization intensities. Parity-violating effects in the early Universe may give rise to a nonzero value of V. By using detectors to measure it, we can extract information about the circular polarization of GWs. We can express GW power spectral density S_{ij} as

$$S_{ij}(f) = I(f)\Gamma^I_{ij}(f) + V(f)\Gamma^V_{ij}(f), \tag{21}$$

where $\Gamma^I_{ij}(f)$ and $\Gamma^V_{ij}(f)$ are the overlap reduction functions for intensity and circular polarization components, quantifying the correlated response between TDI channels i and j. These functions are defined as:

$$\Gamma^I_{ij}(f) = \frac{\Gamma^R_{ij}(f) + \Gamma^L_{ij}(f)}{2},$$
$$\Gamma^V_{ij}(f) = \frac{\Gamma^R_{ij}(f) - \Gamma^L_{ij}(f)}{2}. \tag{22}$$

Thus, the power spectral density in equation (12) for $\tilde{\Gamma}^{\lambda}_{ij}(f)$ can be reformulated using the Stokes parameters I and V, with $\lambda = I, V$. By cross-correlating the signals from LISA and Taiji channels, we can extract nonzero $\tilde{\Gamma}^V_{ij}(f)$ values. The I and V components resulting from this cross-correlation of all TDI channels between LISA and Taiji are presented in figure 4.

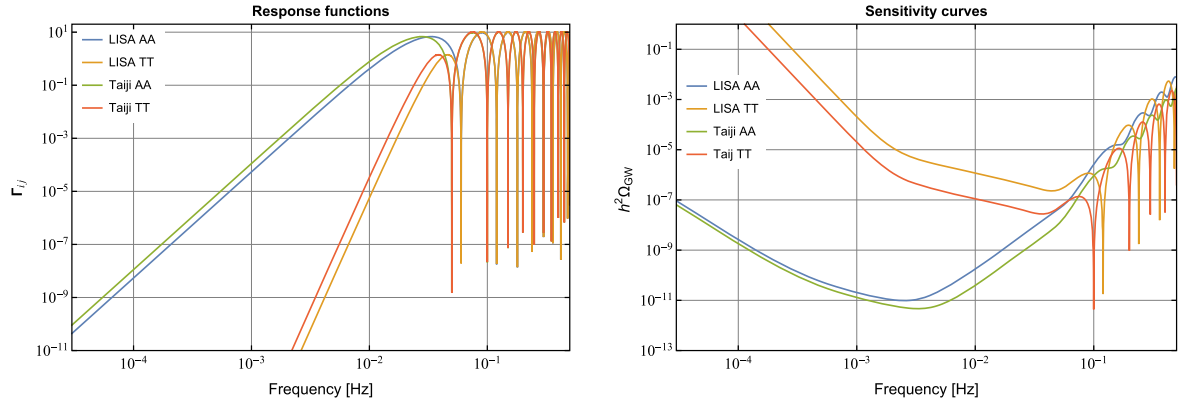

(a) The self-correlation response functions $\Gamma_{ij}(f)$. (b) Sensitivity curves for the total intensity of GWs.

Figure 3. (a) The self-correlation response functions Γ_{ij} in (A14) of a single detector, for the respective TDI channels of LISA and Taiji, where the E-channel has the same result as the A channel. (b) The sensitivity curves for the total intensity of GWs in equation (18) for the self-correlation of the respective channels of LISA and Taiji, where again the E-channel has the same results as the A-channel.

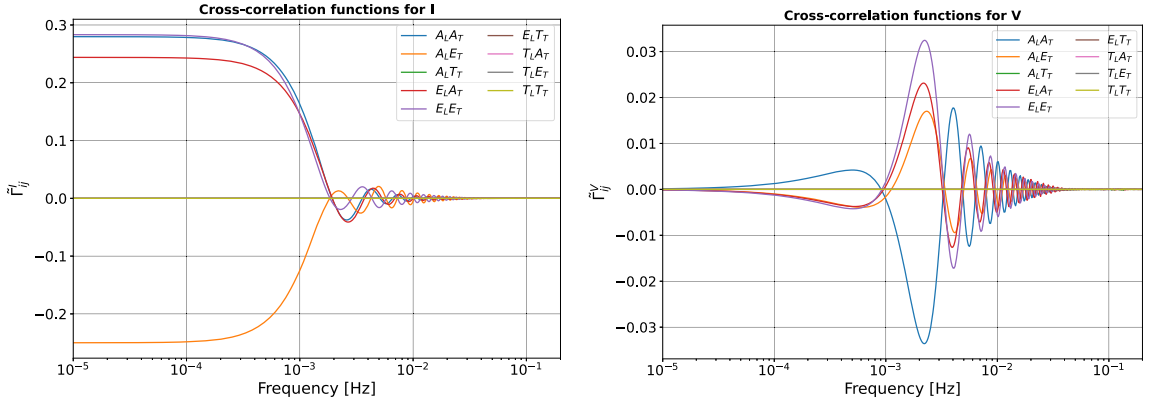

(a) Cross-correlation functions $\tilde{\Gamma}^I_{ij}(f)$ for LISA-Taiji. (b) Cross-correlation functions $\tilde{\Gamma}^V_{ij}(f)$ for LISA-Taiji.

Figure 4. Cross-correlation functions $\tilde{\Gamma}^{\lambda}_{ij}(f)$ in equation (A11) between the TDI channels of LISA and Taiji, for Stokes parameter I in (a) and V in (b).

Additionally, we introduce the circular polarization parameter as

$$\Pi(f) = \frac{V(f)}{I(f)}. \tag{23}$$

The correlation between the outputs of different detectors can be expressed as:

$$\langle \mathcal{C}_{ij} \rangle = \langle \tilde{d}_i \tilde{d}_j \rangle = \frac{1}{2}[\Gamma^I_{ij}(f) I(f) + \Gamma^V_{ij}(f) V(f)]. \tag{24}$$

Assuming that the noise is Gaussian, the likelihood function of the signal model is [98]

$$\mathcal{L} = p(\mathcal{C}|\theta) \propto \exp\left\{-\frac{T_{\rm obs}}{2}\sum_{\kappa}\int_0^{\infty} {\rm d}f \frac{[2\mathcal{C}_{\kappa} - (\Gamma^I_{\kappa} I + \Gamma^V_{\kappa} V)]^2}{N^2_{\kappa}(f)}\right\}, \tag{25}$$

where $\kappa = \{A_L - A_T, A_L - E_T, E_L - A_T, E_L - E_T\}$ represents the independent channel pairs of LISA and Taiji. With A_L and E_L denoting the LISA channels and A_T and E_T corresponding to the Taiji channels. $T_{\rm obs}$ denotes the effective observation time, which is set to 3 years in this work. The noise term $N_{\kappa}(f)$ is defined as $N_{\kappa}(f) = \sqrt{N_i(f) N_j(f)}$. For strong GW signal, such as an SGWB with a large signal-to-noise ratio (SNR), $N^2_{\kappa}(f)$ in (25) is replaced by [98–100]

$$M_{ij}(f) = (N_i + \Gamma_{ii} I)(N_j + \Gamma_{jj} I) + (\Gamma^I_{ij} I + \Gamma^V_{ij} V)^2. \tag{26}$$

4. Fisher matrix analysis

In this section, we employ Fisher matrix analysis to estimate the measurement accuracy of the GW spectral parameters. The Fisher matrix is given by as [61, 98]

$$F_{ab} = -\sum_{\kappa} 4T_{\rm obs}\int_0^{\infty} {\rm d}f \frac{\frac{\partial\langle C_{\kappa}\rangle}{\partial\theta_a}\frac{\partial\langle C_{\kappa}\rangle}{\partial\theta_b}}{N^2_{\kappa}(f)}, \tag{27}$$

where θ_a and θ_b are the model parameters. The term C_{κ} is the correlation of the observed data between the κ channel sets, and $N_{\kappa}(f)$ represents the signal variance caused by noise. For the frequency integration, we take the lower cutoff at 10^{-5} Hz and the upper cutoff at 10^{-1} Hz. In this study, we assume a

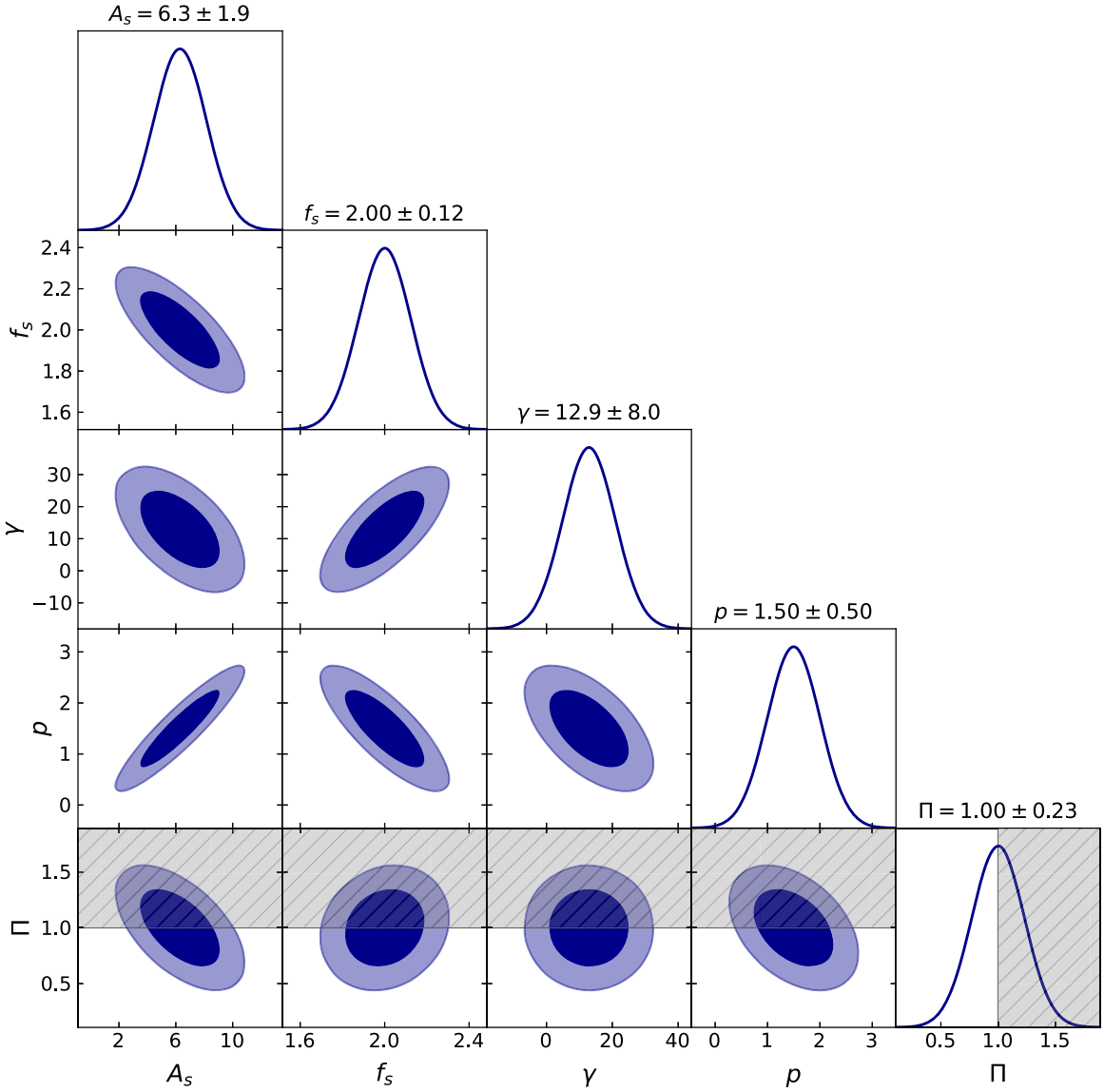

Figure 5. Corner plots of SGWB spectral parameters estimates for the dark photon coupling model derived from the Fisher matrix, with parameter values listed in table 2. At the top of each column, the corresponding parameters' 1σ uncertainty are presented. The gray shaded areas correspond to regions of the parameter space with $\Pi > 1$, which is theoretically unacceptable.

frequency-independent circular polarization parameter $\Pi(f) = \Pi$ and derive the Fisher matrix expression for the GW model parameters as follows.

By substituting the signal equation (19), the circular polarization parameter in equation (23), and equation (24), we have

$$F_{ab} = 4T_{\rm obs}\left(\frac{3H_0^2}{4\pi^2}\right)^2 \times \sum_\kappa \int_0^\infty {\rm d}f \frac{(\Gamma_\kappa^I + \Pi\,\Gamma_\kappa^V)^2 \partial_{\theta_a}\Omega(f)\partial_{\theta_b}\Omega(f)}{f^6\,N_\kappa^2}, \quad (28)$$

with a and b indicate both parameters of the GW model. For example, when one parameter is Π and the other is a GW model parameter

$$F_{a\Pi} = 4T_{\rm obs}\left(\frac{3H_0^2}{4\pi^2}\right)^2 \times \sum_\kappa \int_0^\infty {\rm d}f \frac{\Gamma_\kappa^V(\Gamma_\kappa^I + \Pi\,\Gamma_\kappa^V)\,\Omega(f)\partial_{\theta_a}\Omega(f)}{f^6\,N_\kappa^2}. \quad (29)$$

When both parameters in the Fisher matrix are Π

$$F_{\Pi\Pi} = 4T_{\rm obs}\left(\frac{3H_0^2}{4\pi^2}\right)^2 \sum_\kappa \int_0^\infty {\rm d}f \frac{(\Gamma_\kappa^V)^2\Omega(f)^2}{f^6\,N_\kappa^2}. \quad (30)$$

4.1. GW spectral parameters

We selected the spectral parameters of the GW template for parameter estimation, as detailed in table 2, and the results

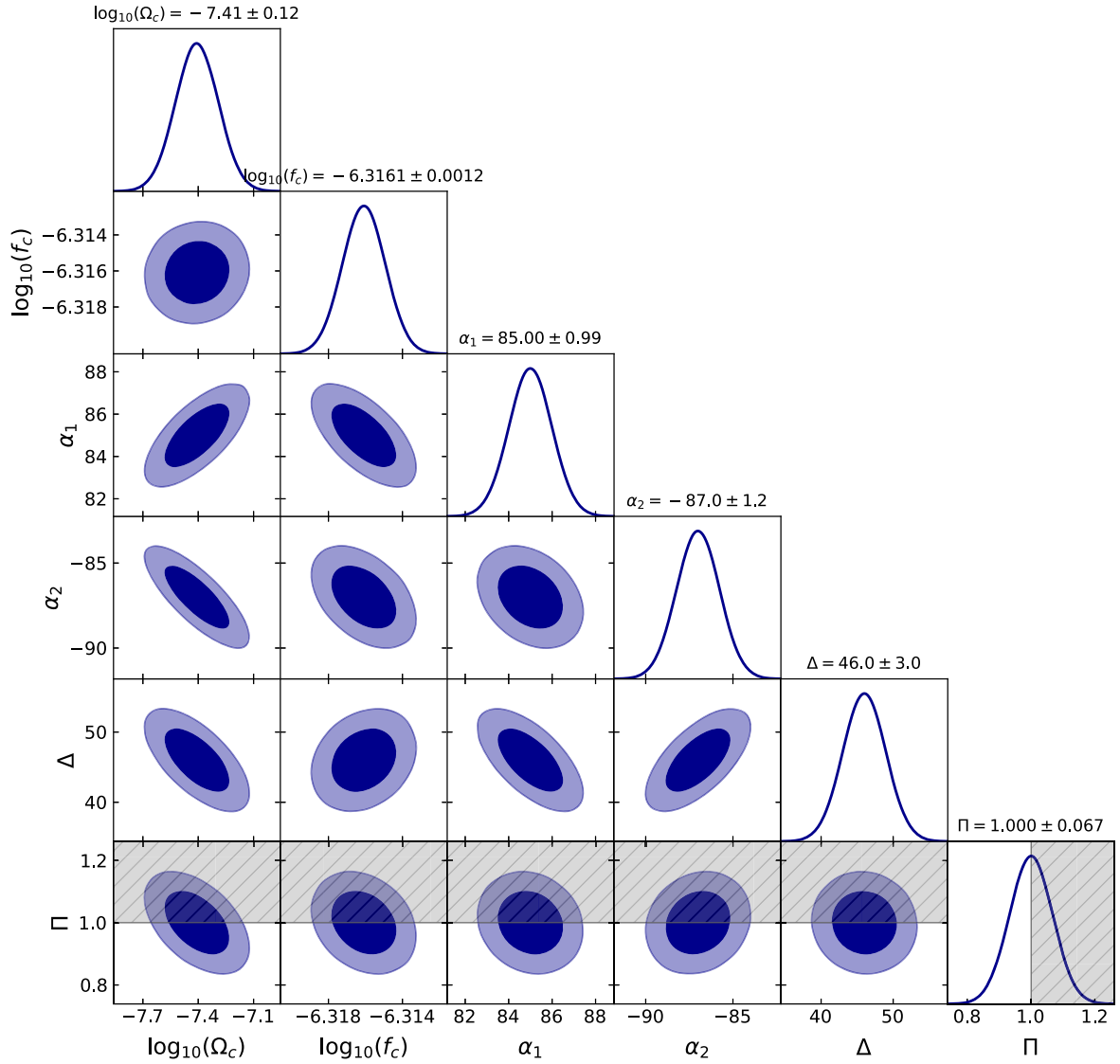

Figure 6. Corner plots of SGWB spectral parameters estimates for the Nieh–Yan coupling model derived from the Fisher matrix, with parameter values listed in table 3. At the top of each column, the corresponding parameters' 1σ uncertainty is presented. The gray shaded areas correspond to regions of the parameter space with $\Pi > 1$, which is theoretically unacceptable.

Table 2. Parameter values for the broken power-law template (2) for the dark photon coupling model.

A_s	f_s	γ	p	Π
6.3	2.0	12.9	1.5	0.9999

from the Fisher analysis of the GW energy density spectrum template (2) for audible axion are illustrated in figure 5. Our nearly maximally polarized signal ($\Pi = 0.9999$) arises from the tachyonic instability due to the axion-like terms in [32, 52], where axion oscillations cause one helicity mode to grow exponentially, generating a highly chiral GW background. Simulations of both dark photon and Nieh–Yan couplings validate this high polarization degree.

For the dark photon coupling model, the uncertainties in the parameter estimates are illustrated graphically, encompassing four spectral parameters $\{A_s, f_s, \gamma, p\}$ and the circular polarization parameter Π. The confidence ellipses indicate that the true parameter values lie within the inner ellipse at a 1σ confidence level and within the outer ellipse at a 2σ confidence level. At the 1σ confidence level, the relative errors are less than 62.0% for spectral parameters and less than 23.0% for Π. The elongation of the confidence ellipses reflects the strength of the correlation among spectral parameters, with more elongated ellipses indicating stronger correlations. Specifically, p and A_s exhibit a strong correlation. Additionally, the Π is negatively correlated with A_s, p, shows a weak negative correlation with γ and is independent of f_s. In figures 5, 6, 7(a), and (b), the gray solid line represents the fiducial value $\Pi = 1$, representing a fully polarized state. The gray shaded areas in the corner plots correspond to regions of the parameter space where $\Pi > 1$, which is theoretically unacceptable.

For the broken power-law template in the Nieh–Yan coupling models, we also have selected the spectral parameters

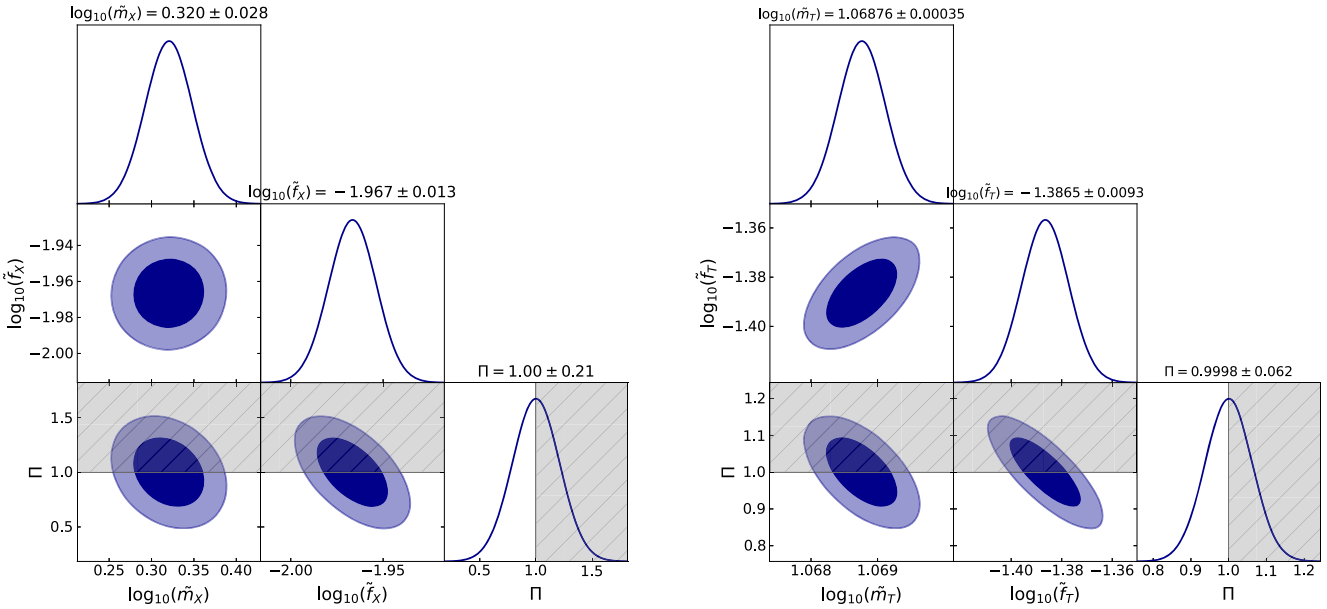

(a) Normalized parameters in dark photon coupling model. (b) Normalized parameters in Nieh-Yan coupling model.

Figure 7. Corner plots showing SGWB normalized model parameters estimates from the Fisher matrix for (a) the dark photon coupling model and (b) the Nieh–Yan coupling model in table 4. At the top of each column, the corresponding parameters' 1σ uncertainties are presented. The gray shaded areas correspond to regions of the parameter space with $\Pi > 1$ which is theoretically unacceptable.

Table 3. Parameter values for the broken power-law template (6) for the Nieh–Yan coupling model.

Ω_c	f_c/mHz	α_1	α_2	Δ	Π
6.072×10^{-4}	1.807	85	−87	46	0.9999

as shown in table 3, with the corresponding Fisher analysis results presented in figure 6. The direct coupling of the axion to the gravitational field in equation (5) and the parameter choices in table 3 result in a strong signal, making the variance assumption invalid. Therefore, the noise term N_κ^2 in our Fisher matrix is replaced by $M_\kappa(f)$ in equation (26). The Fisher analysis results for the GW energy density spectrum in the Nieh–Yan coupling model are shown in figure 6. At the 1σ confidence level, the relative errors are less than 31.8% for spectral parameters and less than 6.7% for Π. Ω_c and f_c exhibit relatively independent errors, while other spectral parameters show significant correlations. Furthermore, the circular polarization parameter Π exhibits a negative correlation with Ω_c and f_c, a statistically weak correlation with α_1 and α_2, and no correlation with Δ.

4.2. Normalized model parameters

Based on the relationship between the spectral parameters and the physical parameters, the equations (3) and (4) for the dark photon couplings, as well as equations (7) and (8) for the Nieh–Yan coupling, which enables us to constrain the physical parameters via measurements of the spectral shape.

We introduce the dimensionless normalized model parameters by combining the axion mass m, the coupling constant $\alpha_{X/T}$, and the decay constant $f_{X/T}$ as follows

$$\tilde{m}_{X/T} = \frac{m}{\mathrm{eV}}\left(\frac{\alpha_{X/T}}{M_P^2}\right)^{4/3}, \tag{31}$$

$$\tilde{f}_X = \frac{f_X}{M_P}\left(\frac{\alpha_X}{M_P^2}\right)^{-\frac{1}{3}}, \qquad \tilde{f}_T = \frac{f_T}{M_P}, \tag{32}$$

and substitute them into the spectral form (2) and (6). From the specific physical parameters of the dark photon coupling and the Nieh–Yan coupling models, as described in sections 2.1 and 2.2 respectively, we obtain the values of these dimensionless normalized model parameters, which are explicitly listed in table 4. We use the Fisher matrix to estimate the normalized model parameters.

Table 4. Values of the normalized model parameters for dark photon coupling and Nieh–Yan coupling models. The subscript $\mathcal{O}$ in $\tilde{m}_\mathcal{O}$ and $\tilde{f}_\mathcal{O}$ denotes the model index: $\mathcal{O} = X$ for dark photon coupling, $\mathcal{O} = T$ for Nieh–Yan coupling.

	$\tilde{m}_\mathcal{O}$	$\tilde{f}_\mathcal{O}$	Π
X(Dark Photon)	2.092	0.0108	0.9999
T(Nieh–Yan)	11.72	0.0411	0.9999

We compute the Fisher matrix of the normalized model parameters $\tilde{m}$, $\tilde{f}_X$, and $\tilde{f}_T$ to obtain its covariance matrix. The correlation plots of this matrix are shown in figures 7(a) and (b). We can constrain the values of the physical parameters by the measurement of these normalized model parameters.

For dark photon coupling model as given in equation (2), the results are shown in figure 7(a). At the 1σ confidence

level, the relative errors are less than 6.7% for the normalized model parameters. It can be observed that the measurements of $\tilde{m}_X$ and $\tilde{f}_X$ are approximately independent, whereas Π exhibits a certain degree of negative correlation with both $\tilde{m}_X$ and $\tilde{f}_X$. The parameter Π is estimated to be 0.9999 with a relative uncertainty of 21.0% at the 1σ confidence level. To improve the measurement precision of Π, we can enhance the sensitivity of individual detectors and the detector network, as well as achieve higher SNR.

For the Nieh–Yan coupling model, the result for the broken power-law template in equation (6) is shown in figure 7. At the 1σ confidence level, the relative errors are less than 2.2% for the normalized model parameters. It can be observed that the measurements of the parameters $\tilde{m}_T$, $\tilde{f}_T$, and Π are correlated. Moreover, due to the strong signal strength, the measurement precision of Π has been improved compared to the results for the dark photon coupling model, with a relative error of 6.2% at the 1σ confidence level. Meanwhile, we can see that the measurement precision of $\tilde{m}_T$ is relatively high. This is because the broken power-law template has a narrow peak and strong amplitude at the peak frequency, measuring the peak frequency more sensitive. According to the relationships (7) and (31), it is clear that $\tilde{m}$ corresponds to the measurement of the peak frequency.

5. Conclusion

The single GW detectors face challenges in detecting the chirality of GWs due to their planar design. However, with the network of space-based detectors such as LISA and Taiji through cross-correlation techniques, we can compute chirality-dependent response functions and extract the net circular polarization of an isotropic SGWB. The detection of parity violation through chiral GWs is crucial for understanding the early Universe and for distinguishing a cosmological GW background from an astrophysical one. In this work, we present the response functions for Stokes parameters I and V, as well as the total intensity sensitivity curve for GWBs originating from audible axions, using the LISA-Taiji network. In addition to the LISA-Taiji network, other space-based GW detector networks such as LISA-TianQin have also been proposed and studied extensively [101–104].

We use the Fisher information matrix to estimate both spectral parameters and normalized model parameters of axion-induced chiral GW spectra through the LISA-Taiji network, focusing on axion-dark photon and axion-Nieh–Yan couplings with physical parameters selected to yield strong GWs in the mHz range. Our results demonstrate that the network estimates the spectral shape parameters and normalized model parameters for both coupling models. For the spectral shape parameters in the dark photon coupling model, we obtain relative errors of 62.0% at the 1σ confidence level, while for the Nieh–Yan coupling model, the relative errors are less than 31.8% at the same confidence level. Regarding circular polarization parameter Π, its relative error is less than 23.0% (1σ) for the dark photon coupling model, and it is reduced to 6.7% (1σ) for the stronger signals from the Nieh–Yan coupling model. Compared to flat GW spectra in [61], we have computed the parameter uncertainties for frequency-dependent spectra of the axion-induced chiral GWB, demonstrating the LISA-Taiji network's capability to effectively constrain both GW spectral parameters and normalized model parameters.

Acknowledgments

This work is supported by the National Key Research and Development Program of China (Grant Nos. 2023YFC 2206200 and 2021YFC2201901) and the National Natural Science Foundation of China (Grant Nos. 12375059 and 12405074).

Appendix. Response functions of GWs

In this work, we employ natural units and adopt the Lorentz transverse-traceless gauge. We establish a coordinate system $\{\hat{e}_x, \hat{e}_y, \hat{e}_z\}$ at rest relative to an isotropic SGWB.

A.1. Polarization tensor bases

For an incoming plane GW with a single wave vector $\overrightarrow{k}$, we define an orthogonal basis

$$\hat{u}(\hat{k}) = \frac{\hat{k} \times \hat{e}_z}{|\hat{k} \times \hat{e}_z|}, \quad \hat{v}(\hat{k}) = \hat{k} \times \hat{u}, \tag{A1}$$

where $\hat{k}$ denotes the unit vector in the direction of wave-vector $\overrightarrow{k}$, and its magnitude is given by $k = |\overrightarrow{k}|$. Using the above equation, we define the so-called 'plus' (+) and 'cross' (×) polarization tensors as

$$e^{+}_{ab}(\hat{k}) = \frac{\hat{u}_a\hat{u}_b - \hat{v}_a\hat{v}_b}{\sqrt{2}}, \quad e^{\times}_{ab}(\hat{k}) = \frac{\hat{u}_a\hat{v}_b + \hat{v}_a\hat{u}_b}{\sqrt{2}}. \tag{A2}$$

It is more convenient to introduce the circular polarization basis tensors e^{R}_{ab} and e^{L}_{ab} when searching for evidence of circular polarization in the background. Then the relationships between the left- and right-handed polarization tensors and the 'plus' (+) and 'cross' (×) polarization basis are

$$e^{R}_{ab}(\hat{k}) = \frac{e^{+}_{ab} + \mathrm{i}e^{\times}_{ab}}{\sqrt{2}}, \quad e^{L}_{ab}(\hat{k}) = \frac{e^{+}_{ab} - \mathrm{i}e^{\times}_{ab}}{\sqrt{2}}. \tag{A3}$$

The superposition of GWs arriving at position $\overrightarrow{x}$ at time t can be represented as an incident plane wave

$$h_{ab}(\overrightarrow{x}, t) = \int_{-\infty}^{+\infty} \mathrm{d}f \int_{\Omega} \mathrm{d}\Omega_{\hat{k}}\, \mathrm{e}^{2\pi \mathrm{i} f(t-\hat{k}\cdot\overrightarrow{x})} \sum_{P} \tilde{h}_P(f, \hat{k}) e^{P}_{ab}(\hat{k}), \tag{A4}$$

where the index P labels either the plus and cross polarizations (+/×) or the left- and right-handed polarizations (L/R). Here, $f = k\,c$ denotes the frequency of each plane wave, $\mathrm{d}\Omega_{\hat{k}}$ represents the infinitesimal solid angle corresponding to the wave vector $\overrightarrow{k}$, and $\tilde{h}_P(f, \hat{k}) \equiv f^2 \tilde{h}_P(\overrightarrow{k})$. Finally, the

gravitational wave can be expressed in terms of $\overrightarrow{k}$ as

$$h_{ab}(\overrightarrow{x},t)=\int \mathrm{d}^3k\ \mathrm{e}^{-2\pi \mathrm{i}\overrightarrow{k}\cdot\overrightarrow{x}}\sum_P[\mathrm{e}^{2\pi \mathrm{i}kt}\tilde{h}_P(\overrightarrow{k})e^P_{ab}(\hat{k}) + \mathrm{e}^{-2\pi \mathrm{i}kt}\tilde{h}^*_P(-\overrightarrow{k})e^{P*}_{ab}(-\hat{k})]. \tag{A5}$$

A.2. Quadratic response functions

In actual measurements, space-based detectors measure differential Doppler frequency shifts rather than direct time shifts. These shifts are defined as $\Delta F_{12}(t)\equiv\Delta\nu_{12}(t)/\nu=-d\Delta T_{12}(t)/dt$. We use L to denote the detector arm length. The most straightforward interferometric measurement at a vertex performed by a space-based detector is

$$\Delta F_{1(23)}(t)=\Delta F_{21}(t-L)+\Delta F_{12}(t) - [\Delta F_{31}(t-L)+\Delta F_{13}(t)]. \tag{A6}$$

In order to suppress noise induced by laser phase variations and other factors, we implement TDI techniques. Consider two test masses labeled i and j, and let $\hat{l}_{ij}=(\boldsymbol{x}_j-\boldsymbol{x}_i)/|\boldsymbol{x}_j-\boldsymbol{x}_i|$ denote the unit vector pointing from mass i to mass j among the three detector spacecraft. The TDI1.5 variable is obtained through cyclic permutation of the TDI variables Y and Z

$$\begin{aligned}\Delta F^{1.5}_{1(23)}(t)&=\Delta F_{1(23)}(t-2L)+\Delta F_{1(32)}(t)\\ =&-\int \mathrm{d}^3k\ \mathrm{e}^{-2\pi \mathrm{i}\overrightarrow{k}\cdot\overrightarrow{x_1}}(2\pi \mathrm{i}kL)\\ &\times\sum_\lambda[\mathrm{e}^{2\pi \mathrm{i}k(t-L)}W(kL)R^\lambda_1(\overrightarrow{k},\hat{l}_{12},\hat{l}_{13})\tilde{h}_\lambda(k)\\ &-\mathrm{e}^{-2\pi \mathrm{i}k(t-L)}W^*(kL)R^{\lambda^*}_1(-\overrightarrow{k},\hat{l}_{12},\hat{l}_{13})\tilde{h}^*_\lambda(-k)].\end{aligned} \tag{A7}$$

where $\lambda=L$ or R denotes left- and right-handed polarizations, and $W(kL)\equiv\mathrm{e}^{-4\pi \mathrm{i}kL}-1$. The function R^λ_i is defined as

$$R^\lambda_i(\overrightarrow{k},\hat{l}_{ij},\hat{l}_{ik})\equiv\frac{\hat{l}^a_{ij}\hat{l}^b_{ij}}{2}e^\lambda_{ab}(\hat{k})\mathcal{T}(\overrightarrow{k},\hat{l}_{ij})-\frac{\hat{l}^a_{ik}\hat{l}^b_{ik}}{2}e^\lambda_{ab}(\hat{k})\mathcal{T}(\overrightarrow{k},\hat{l}_{ik}), \tag{A8}$$

where the detector transfer function $\mathcal{T}(\overrightarrow{k},\hat{l}_{ij})$ is given by

$$\mathcal{T}(\overrightarrow{k},\hat{l}_{ij})\equiv\mathrm{e}^{\pi \mathrm{i}kL(1-\hat{k}\cdot\hat{l}_{ij})}\mathrm{sinc}[\pi kL(1+\hat{k}\cdot\hat{l}_{ij})] + \mathrm{e}^{-\pi \mathrm{i}kL(1+\hat{k}\cdot\hat{l}_{ij})}\mathrm{sinc}[\pi kL(1-\hat{k}\cdot\hat{l}_{ij})]. \tag{A9}$$

For simplicity, we represent the detector output using the notation $s_i(t)\equiv\Delta F^{1.5}_{i(jk)}(t)$. The information is contained within the two-point correlation functions of the data streams. Below, without assuming identical detectors, we present the general formulation. The two-point cross-correlation is expressed as

$$\langle s_i(t)s_j(t)\rangle=\int \mathrm{d}k\ (2\pi kL_i)(2\pi kL_j)\sum_\lambda P_\lambda(k) \times[\mathrm{e}^{-2\pi \mathrm{i}k(L_i-L_j)}W(kL_i)W^*(kL_j)\tilde{\Gamma}^\lambda_{ij}(k)+\mathrm{h.c.}], \tag{A10}$$

where the cross-correlation function

$$\tilde{\Gamma}^\lambda_{ij}(k)\equiv\frac{1}{4\pi}\int \mathrm{d}^2\hat{k}\ \mathrm{e}^{-2\pi \mathrm{i}\overrightarrow{k}\cdot(\overrightarrow{x_i}-\overrightarrow{x_j})} \times R^\lambda_i(\overrightarrow{k},\hat{l}_{ik},\hat{l}_{il})R^{\lambda^*}_j(\overrightarrow{k},\hat{l}_{jm},\hat{l}_{jn}). \tag{A11}$$

Table 5. Summary of the symbols and descriptions.

Symbols	Descriptions
$S_{ij}(f)$	One-sided signal power spectral density
$N_i(f)$	One-sided noise power spectral density
$h_{ab}(\overrightarrow{x},t)$	Gravitational wave strain tensor
$\Delta F_{ij}(t)$	Doppler frequency shifts
$\tilde{\Gamma}^\lambda_{ij}(k)$	Cross-correlation function
$\Gamma^\lambda_{ij}(k)$	Quadratic response function

For notational simplicity, the quadratic response function

$$\Gamma^\lambda_{ij}(k)\equiv(2\pi kL_i)(2\pi kL_j)W(kL_i)W^*(kL_j)\tilde{\Gamma}^\lambda_{ij}(k)+\mathrm{h.c.}, \tag{A12}$$

we obtain the compact form

$$\langle s_i(t)s_j(t)\rangle=\int \mathrm{d}k[\Gamma^L_{ij}(k)P_L(k)+\Gamma^R_{ij}(k)P_R(k)]. \tag{A13}$$

When i and j are both LISA (or Taiji) channels, the response function is given by

$$\begin{aligned}\Gamma_{ij}(k)&=\Gamma^L_{ij}(k)+\Gamma^R_{ij}(k)\\ &=16(2\pi kL)^2\sin^2(2\pi kL)\tilde{\Gamma}_{ij}(k),\end{aligned} \tag{A14}$$

where $\tilde{\Gamma}_{ij}(k)=\tilde{\Gamma}^L_{ij}(k)=\tilde{\Gamma}^R_{ij}(k)$ [13]. The response functions Γ_{ij} for the A and E channels of LISA and Taiji are shown in figure 3(a).

Using the methods in [61, 105], we have calculated the response functions and total intensity sensitivity curves associated with the self-correlation of LISA and Taiji. The corresponding results are shown in figure 3. Additionally, we have obtained the response functions for the I and V components of all cross-correlation TDI channels between LISA and Taiji, as shown in figure 4. For further details on the derivation, we refer to [13, 61].

A.3. The AET bases

In space-based gravitational wave detection, the fundamental TDI channels of a Michelson interferometer include X, Y, and Z. We transform the X, Y, and Z channels into the noise-independent channels A, E, and T, which are related as follows [61]

$$\tilde{d}_A=\frac{1}{\sqrt{2}}(\tilde{d}_Z-\tilde{d}_X), \tag{A15}$$

$$\tilde{d}_E=\frac{1}{\sqrt{6}}(\tilde{d}_X-2\tilde{d}_Y+\tilde{d}_Z), \tag{A16}$$

$$\tilde{d}_T=\frac{1}{\sqrt{3}}(\tilde{d}_X+\tilde{d}_Y+\tilde{d}_Z). \tag{A17}$$

The noise independence of the A, E, and T channels is valid under the assumptions of identical noise in each laser link and equal arm lengths.

For convenience, we summarize the key symbols used in this paper in table 5.

ORCID iDs

Ju Chen https://orcid.org/0000-0002-2461-0693
Chang Liu https://orcid.org/0000-0002-3111-5957
Yun-Long Zhang https://orcid.org/0000-0002-7225-8479

References

[1] Abbott B P *et al* (LIGO Scientific, Virgo) 2016 Observation of gravitational waves from a binary black hole merger *Phys. Rev. Lett.* **116** 061102
[2] Abramovici A *et al* 1992 LIGO: the Laser interferometer gravitational wave observatory *Science* **256** 325
[3] Allen B 1996 The stochastic gravity wave background: sources and detection *Les Houches School of Physics: Astrophysical Sources of Gravitational Radiation* 373–417
[4] Maggiore M 2000 Gravitational wave experiments and early universe cosmology *Phys. Rept.* **331** 283
[5] Kuroyanagi S, Chiba T and Takahashi T 2018 Probing the universe through the stochastic gravitational wave background *J. Cosmol. Astropart. Phys.* **11** 038
[6] Auclair P *et al* (LISA Cosmology Working Group) 2023 Cosmology with the Laser Interferometer Space Antenna *Living Rev. Rel.* **26** 5
[7] Binetruy P, Bohe A, Caprini C and Dufaux J-F 2012 Cosmological backgrounds of gravitational waves and eLISA/NGO: phase transitions, cosmic strings and other sources *J. Cosmol. Astropart. Phys.* **06** 027
[8] Thrane E and Romano J D 2013 Sensitivity curves for searches for gravitational-wave backgrounds *Phys. Rev.* D **88** 124032
[9] Romano J D and Cornish N J 2017 Detection methods for stochastic gravitational-wave backgrounds: a unified treatment *Living Rev. Rel.* **20** 2
[10] Caprini C and Figueroa D G 2018 Cosmological backgrounds of gravitational waves *Class. Quantum Grav.* **35** 163001
[11] Cheng S-L, Lee W and Ng K-W 2018 Primordial black holes and associated gravitational waves in axion monodromy inflation *J. Cosmol. Astropart. Phys.* **07** 001
[12] Boileau G, Christensen N, Meyer R and Cornish N J 2021 Spectral separation of the stochastic gravitational-wave background for LISA: Observing both cosmological and astrophysical backgrounds *Phys. Rev.* D **103** 103529
[13] Flauger R, Karnesis N, Nardini G, Pieroni M, Ricciardone A and Torrado J 2021 Improved reconstruction of a stochastic gravitational wave background with LISA *J. Cosmol. Astropart. Phys.* **2021** 059
[14] van Remortel N, Janssens K and Turbang K 2023 Stochastic gravitational wave background: methods and implications *Prog. Part. Nucl. Phys.* **128** 104003
[15] Peccei R D and Quinn H R 1977 CP Conservation in the Presence of Instantons *Phys. Rev. Lett.* **38** 1440
[16] Peccei R D and Quinn H R 1977 Constraints imposed by CP conservation in the presence of instantons *Phys. Rev.* D **16** 1791
[17] Weinberg S 1978 A new light boson? *Phys. Rev. Lett.* **40** 223
[18] Wilczek F 1978 Problem of strong *P* and *T* invariance in the presence of instantons *Phys. Rev. Lett.* **40** 279
[19] Du N *et al* (ADMX) 2018 A search for invisible axion dark matter with the axion dark matter experiment *Phys. Rev. Lett.* **120** 151301
[20] Di Luzio L, Giannotti M, Nardi E and Visinelli L 2020 The landscape of QCD axion models *Phys. Rept.* **870** 1
[21] Abbott L F and Sikivie P 1983 A cosmological bound on the invisible axion *Phys. Lett.* B **120** 133
[22] Ipser J and Sikivie P 1983 Are galactic halos made of axions? *Phys. Rev. Lett.* **50** 925
[23] Marsh D J E 2016 Axion cosmology *Phys. Rept.* **643** 1
[24] Preskill J, Wise M B and Wilczek F 1983 Cosmology of the invisible axion *Phys. Lett.* B **120** 127
[25] Sikivie P 1983 Experimental tests of the invisible axion *Phys. Rev. Lett.* **51** 1415
[26] Georgi H, Quinn H R and Weinberg S 1974 Hierarchy of interactions in unified gauge theories *Phys. Rev. Lett.* **33** 451
[27] Graham P W, Kaplan D E and Rajendran S 2015 Cosmological relaxation of the electroweak scale *Phys. Rev. Lett.* **115** 221801
[28] Dine M and Fischler W 1983 The not-so-harmless axion *Phys. Lett.* B **120** 137
[29] Bertone G and Hooper D 2018 History of dark matter *Rev. Mod. Phys.* **90** 045002
[30] Freese K, Frieman J A and Olinto A V 1990 Natural inflation with pseudo Nambu–Goldstone bosons *Phys. Rev. Lett.* **65** 3233
[31] Arvanitaki A, Dimopoulos S, Dubovsky S, Kaloper N and March-Russell J 2010 String axiverse *Phys. Rev.* D **81** 123530
[32] Machado C S, Ratzinger W, Schwaller P and Stefanek B A 2019 Audible axions *J. High Energy Phys.* **01** 053
[33] Madge E, Ratzinger W, Schmitt D and Schwaller P 2022 Audible axions with a booster: stochastic gravitational waves from rotating ALPs *SciPost Phys.* **12** 171
[34] Lue A, Wang L-M and Kamionkowski M 1999 Cosmological signature of new parity violating interactions *Phys. Rev. Lett.* **83** 1506
[35] Nagano K, Fujita T, Michimura Y and Obata I 2019 Axion dark matter search with interferometric gravitational wave detectors *Phys. Rev. Lett.* **123** 111301
[36] Heinze J, Gill A, Dmitriev A, Smetana J, Yan T, Boyer V, Martynov D and Evans M 2024 First results of the laser-interferometric detector for axions (LIDA) *Phys. Rev. Lett.* **132** 191002
[37] Yao Y-H and Tang Y 2024 Probing stochastic ultralight dark matter with space-based gravitational-wave interferometers *Phys. Rev.* D **110** 095015
[38] Gué J, Hees A and Wolf P 2025 Probing the axion–photon coupling with space-based gravitational wave detectors *Class. Quantum Grav.* **42** 055015
[39] Yao Y-H, Jiang T and Tang Y 2025 Prospects for axion dark matter searches at LISA-like interferometers *Phys. Rev.* D **111** 055031
[40] Christensen N 2019 Stochastic gravitational wave backgrounds *Rept. Prog. Phys.* **82** 016903
[41] Allen B and Romano J D 1999 Detecting a stochastic background of gravitational radiation: signal processing strategies and sensitivities *Phys. Rev.* D **59** 102001
[42] Jackiw R and Pi S Y 2003 Chern–Simons modification of general relativity *Phys. Rev.* D **68** 104012
[43] Alexander S and Yunes N 2009 Chern–Simons modified general relativity *Phys. Rept.* **480** 1
[44] Li M, Rao H and Zhao D 2020 A simple parity violating gravity model without ghost instability *J. Cosmol. Astropart. Phys.* **2020** 023
[45] Li M, Rao H and Tong Y 2021 Revisiting a parity violating gravity model without ghost instability: local lorentz covariance *Phys. Rev.* D **104** 084077
[46] Cai R-G, Fu C and Yu W-W 2022 Parity violation in stochastic gravitational wave background from inflation in Nieh–Yan modified teleparallel gravity *Phys. Rev.* D **105** 103520

[47] Wu Q, Zhu T, Niu R, Zhao W and Wang A 2022 Constraints on the Nieh–Yan modified teleparallel gravity with gravitational waves *Phys. Rev.* D **105** 024035

[48] Li M and Rao H 2023 Irregular universe in the Nieh–Yan modified teleparallel gravity *Phys. Lett. B* **841** 137929

[49] Li M, Tong Y and Zhao D 2022 Possible consistent model of parity violations in the symmetric teleparallel gravity *Phys. Rev.* D **105** 104002

[50] Rao H and Zhao D 2023 Parity violating scalar-tensor model in teleparallel gravity and its cosmological application *J. High Energy Phys.* **070**

[51] Zhang F, Feng J-X and Gao X 2024 Scalar induced gravitational waves in metric teleparallel gravity with the Nieh–Yan term *Phys. Rev.* D **110** 023537

[52] Xu B, Ding K, Su H, Chen J and Zhang Y-L 2024 Chiral gravitational wave background from audible axion via Nieh–Yan term arXiv:2411.08691

[53] Seto N and Taruya A 2007 Measuring a parity violation signature in the early universe via ground-based laser interferometers *Phys. Rev. Lett.* **99** 121101

[54] Seto N and Taruya A 2008 Polarization analysis of gravitational-wave backgrounds from the correlation signals of ground-based interferometers: measuring a circular-polarization mode *Phys. Rev.* D **77** 103001

[55] Smith T L and Caldwell R 2017 Sensitivity to a frequency-dependent circular polarization in an isotropic stochastic gravitational wave background *Phys. Rev.* D **95** 044036

[56] Martinovic K, Badger C, Sakellariadou M and Mandic V 2021 Searching for parity violation with the LIGO-Virgo-KAGRA network *Phys. Rev.* D **104** L081101

[57] Jiang Y and Huang Q-G 2023 Upper limits on the polarized isotropic stochastic gravitational-wave background from advanced LIGO-Virgo's first three observing runs *J. Cosmol. Astropart. Phys.* **02** 026

[58] Omiya H and Seto N 2023 Measuring the maximally allowed polarization states of the isotropic stochastic gravitational wave background with the ground-based detectors *Phys. Rev.* D **107** 124027

[59] Seto N 2006a Prospects for direct detection of circular polarization of gravitational-wave background *Phys. Rev. Lett.* **97** 151101

[60] Seto N 2020a Gravitational wave background search by correlating multiple triangular detectors in the mHz band *Phys. Rev.* D **102** 123547

[61] Orlando G, Pieroni M and Ricciardone A 2021 Measuring parity violation in the stochastic gravitational wave background with the LISA-Taiji network *J. Cosmol. Astropart. Phys.* **03** 069

[62] Saito S, Ichiki K and Taruya A 2007 Probing polarization states of primordial gravitational waves with CMB anisotropies *J. Cosmol. Astropart. Phys.* **09** 002

[63] Sorbo L 2011 Parity violation in the Cosmic Microwave Background from a pseudoscalar inflaton *J. Cosmol. Astropart. Phys.* **06** 003

[64] Amaro-Seoane P (LISA) *et al* 2017 Laser interferometer space antenna arXiv:1702.00786

[65] Ruan W-H, Guo Z-K, Cai R-G and Zhang Y-Z 2020a Taiji program: gravitational-wave sources *Int. J. Mod. Phys. A* **35** 2050075

[66] Seto N 2006b Correlation analysis of stochastic gravitational wave background around 0.1-1 Hz *Phys. Rev.* D **73** 063001

[67] Abbott B *et al* (LIGO Scientific) 2007 Searching for a stochastic background of gravitational waves with LIGO *Astrophys. J.* **659** 918

[68] Schutz B F 2011 Networks of gravitational wave detectors and three figures of merit *Class. Quantum Grav.* **28** 125023

[69] Seto N 2020b Measuring parity asymmetry of gravitational wave backgrounds with a heliocentric detector network in the mHz band *Phys. Rev. Lett.* **125** 251101

[70] Ruan W-H, Liu C, Guo Z-K, Wu Y-L and Cai R-G 2020b The LISA-Taiji network *Nature Astron.* **4** 108

[71] Wang G, Ni W-T, Han W-B, Xu P and Luo Z 2021 Alternative LISA-Taiji networks *Phys. Rev.* D **104** 024012

[72] Wang G and Han W-B 2021a Alternative LISA-TAIJI networks: detectability of the isotropic stochastic gravitational wave background *Phys. Rev.* D **104** 104015

[73] Liu G-C and Ng K-W 2023 Overlap reduction functions for a polarized stochastic gravitational-wave background in the Einstein telescope-cosmic explorer and the LISA-Taiji networks *Phys. Rev.* D **107** 104040

[74] Cai R-G, Guo Z-K, Hu B, Liu C, Lu Y, Ni W-T, Ruan W-H, Seto N, Wang G and Wu Y-L 2024 On networks of space-based gravitational-wave detectors *Fund. Res.* **4** 1072

[75] Zhao Z-C and Wang S 2024 Measuring the anisotropies in astrophysical and cosmological gravitational-wave backgrounds with Taiji and LISA networks *Sci. China Phys. Mech. Astron.* **67** 120411

[76] Chen J, Liu C and Zhang Y-L 2024a Parity-violating gravitational wave background search with a network of space-borne triangular detectors arXiv:2410.18916

[77] Wang G and Han W-B 2021b Observing gravitational wave polarizations with the LISA-Taiji network *Phys. Rev.* D **103** 064021

[78] Zhang X-H, Zhao S-D, Mohanty S D and Liu Y-X 2022a Resolving Galactic binaries using a network of space-borne gravitational wave detectors *Phys. Rev.* D **106** 102004

[79] Zhang C, Gong Y and Zhang C 2022b Source localizations with the network of space-based gravitational wave detectors *Phys. Rev.* D **106** 024004

[80] Shuman K J and Cornish N J 2022 Massive black hole binaries and where to find them with dual detector networks *Phys. Rev.* D **105** 064055

[81] Ruan W-H, Liu C, Guo Z-K, Wu Y-L and Cai R-G 2021 The LISA-Taiji network: precision localization of coalescing massive black hole binaries *Research* **2021** 6014164

[82] Yang Y, Han W-B, Yun Q, Xu P and Luo Z 2022 Tracing astrophysical black hole seeds and primordial black holes with LISA-Taiji network *Mon. Not. Roy. Astron. Soc.* **512** 6217

[83] Chen J, Yan C-S, Lu Y-J, Zhao Y-T and Ge J-Q 2021 On detecting stellar binary black holes via the LISA-Taiji network *Res. Astron. Astrophys.* **21** 285

[84] Yang T 2021 Gravitational-wave detector networks: standard sirens on cosmology and modified gravity theory *J. Cosmol. Astropart. Phys.* **05** 044

[85] Wang L-F, Jin S-J, Zhang J-F and Zhang X 2022a Forecast for cosmological parameter estimation with gravitational-wave standard sirens from the LISA-Taiji network *Sci. China Phys. Mech. Astron.* **65** 210411

[86] Wang R, Ruan W-H, Yang Q, Guo Z-K, Cai R-G and Hu B 2022b Hubble parameter estimation via dark sirens with the LISA-Taiji network *Natl. Sci. Rev.* **9** nwab054

[87] Machado C S, Ratzinger W, Schwaller P and Stefanek B A 2020 Gravitational wave probes of axionlike particles *Phys. Rev.* D **102** 075033

[88] Salehian B, Gorji M A, Mukohyama S and Firouzjahi H 2021 Analytic study of dark photon and gravitational wave production from axion *J. High Energy Phys.* **2021** 043

[89] Sun S and Zhang Y-L 2021 Fast gravitational wave bursts from axion clumps *Phys. Rev.* D **104** 103009

[90] Li M, Sun S, Yan Q-S and Zhao Z 2024 Gravitational waves from axion wave production *Eur. Phys. J.* C **84** 1165

[91] Ding K, Fu C, Xu B and Zhang Y-L 2024 Chiral gravitational wave background in millihertz from axion-like fields *Sci. Sinica Phys.* **54** 270408

[92] Babak S and Petiteau A 2020 LISA Data Challenge Manual *APC Paris* LISA-LCST-SGS-MAN-002 https://lisa-ldc.lal.in2p3.fr/static/data/pdf/LDC-manual-002.pdf

[93] Armano M *et al* 2016 Sub-femto-*g* free fall for space-based gravitational wave observatories: LISA pathfinder results *Phys. Rev. Lett.* **116** 231101
[94] Babak S, Petiteau A and Hewitson M 2021 LISA Sensitivity and SNR Calculations arXiv:2108.01167
[95] Luo Z, Guo Z, Jin G, Wu Y and Hu W 2020 A brief analysis to Taiji: science and technology *Res. Phys.* **16** 102918
[96] Luo Z, Wang Y, Wu Y, Hu W and Jin G 2021 The Taiji program: a concise overview *PTEP* **2021** 05A108
[97] Prince T A, Tinto M, Larson S L and Armstrong J W 2002 The LISA optimal sensitivity *Phys. Rev.* D **66** 122002
[98] Chen J, Liu C, Zhang Y-L and Wang G 2024 Alternative LISA-Taiji networks: detectability of the parity violation in stochastic gravitational wave background arXiv:2412.18420
[99] Cornish N J and Larson S L 2001 Space missions to detect the cosmic gravitational wave background *Class. Quantum Grav.* **18** 3473
[100] Cornish N J 2002 Detecting a stochastic gravitational wave background with the Laser Interferometer Space Antenna *Phys. Rev.* D **65** 022004
[101] Gong Y, Luo J and Wang B 2021 Concepts and status of Chinese space gravitational wave detection projects *Nature Astron.* **5** 881
[102] Li E-K *et al* 2023 GWSpace: a multi-mission science data simulator for space-based gravitational wave detection arXiv:2309.15020
[103] Wu J and Li J 2023 Subtraction of the confusion foreground and parameter uncertainty of resolvable galactic binaries on the networks of space-based gravitational-wave detectors *Phys. Rev.* D **108** 124047
[104] Luo J *et al* 2025 Fundamental physics and cosmology with TianQin arXiv:2502.20138
[105] Robson T, Cornish N J and Liu C 2019 The construction and use of LISA sensitivity curves *Class. Quantum Grav.* **36** 105011